Room-Temperature Ionic Liquids: Slow Dynamics, Viscosity, and the Red Edge Effect

ZHONGHAN HU AND CLAUDIO J. MARGULIS*

Department of Chemistry, University of Iowa, Iowa City, Iowa 52242

Received March 1, 2007

ABSTRACT

Ionic liquids (ILs) have recently attracted significant attention from academic and industrial sources. This is because, while their vapor pressures are negligible, many of them are liquids at room temperature and can dissolve a wide range of polar and nonpolar organic and inorganic molecules. In this Account, we discuss the progress of our laboratory in understanding the dynamics, spectroscopy, and fluid dynamics of selected imidazolium-based ILs using computational and analytical tools that we have recently developed. Our results indicate that the red edge effect, the non-Newtonian behavior, and the existence of locally heterogeneous environments on a time scale relevant to chemical and photochemical reactivity are closely linked to the viscosity and highly structured character of these liquids.

Introduction

The reason why room-temperature ionic liquids (RTILs) are liquid at room temperature is still not fully understood. From recent X-ray crystal structure studies, we know that some tend to crystallize into disordered solids[1] and, depending upon the rate of cooling, crystal polymorphism[2] can be observed. On the basis of these observations, it has been speculated that the gain in energy upon formation of the crystal is not as large as in traditional inorganic salts and is not enough to compensate for the loss in entropy that accompanies the formation of the crystal at room temperature.[1] Experiments show that several of these systems have a tendency toward glassy behavior[3,4] and, depending upon the length of alkyl substituents in the cations, their properties range from those of normal liquids to glassy or even liquid crystals.[5] As recently discussed in an interesting review article by MacFarlane and co-workers,[6] the possible number of compounds expected to form RTILs is extremely large. Only a very small fraction of these have been synthesized. Their selectivity as media for chemical and photochemical reactions remains *terra incognita* and invites for a thorough theoretical understanding of the trends to be anticipated as molecular modifications are applied.

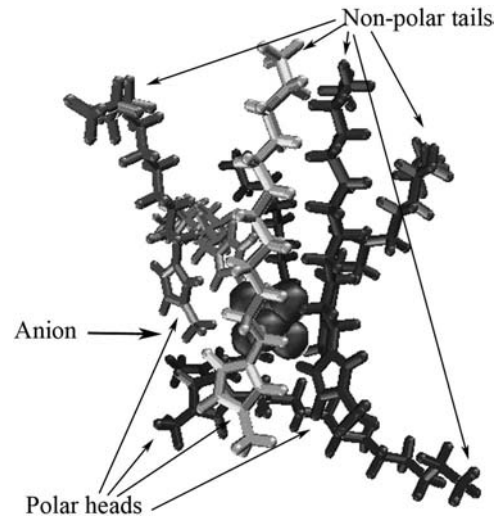

FIGURE 1. Structural heterogeneity. Typical structure found in our simulations of ILs that is reminiscent of a reverse micelle. A spherical [$PF6^-$] anion is in the center (space-filled representation); cationic polar heads surround the anion; and cationic long aliphatic tails point outward. Cation = 1-dodecyl-3-methylimidazolium.

Structural and Dynamical Heterogeneity

To understand the underlying physics behind recent experimental findings in which the slow dynamics of RTILs manifests,[7–17] it is fundamentally important to address the problem of heterogeneity on a time scale relevant to chemical and photochemical reactivity. Dynamical heterogeneity (defined in this Account as non-Gaussian translational and rotational diffusion) can be present in systems that are either structurally homo- or heterogeneous. As an example, supercooled water is structurally homogeneous but clearly shows dynamical heterogeneity.[18–21] On the contrary, colloidal gels are structurally heterogeneous but can also display dynamical heterogeneity.[22–26]

Signs of structural heterogeneity (in this case, the existence of polar and nonpolar environments in certain ILs) have recently been reported in the literature.[27,28] In 2004, we studied[29] a family of imidazolium-based ILs and found that in those with larger alkyl tails, structures reminiscent of reverse micelles, such as that shown in Figure 1, could be detected.

This structural heterogeneity may be important when trying to rationalize why these liquids are able to dissolve a wide range of molecules, ranging from water to cellulose.[30–32] Furthermore, the concept of liquid polarity should also be used carefully because it is possible that polar and nonpolar local environments coexist in the liquid.

It is important to emphasize that a liquid may only show signs of dynamical heterogeneity on a certain time

Zhonghan Hu received his B.S. degree in chemical physics in 2003 from the University of Science and Technology of China in Hefei, People's Republic of China. He is currently a Research Assistant at the University of Iowa.

Claudio J. Margulis received his Licenciado en Ciencias Químicas degree (1996) from The University of Buenos Aires in Argentina and his Ph.D. degree (2001) from Boston University. He joined The University of Iowa as an Assistant Professor in 2003 following postdoctoral studies at Columbia University in New York City. His research interests involve room-temperature ionic liquids, the sugar-folding problem, surface atmospheric problems, and the diffusion of molecules in crowded environments.

* To whom correspondence should be addressed. Fax: 319-335-1270. E-mail: claudio-margulis@uiowa.edu.

10.1021/ar700046m CCC: $37.00
Published on Web 07/28/2007

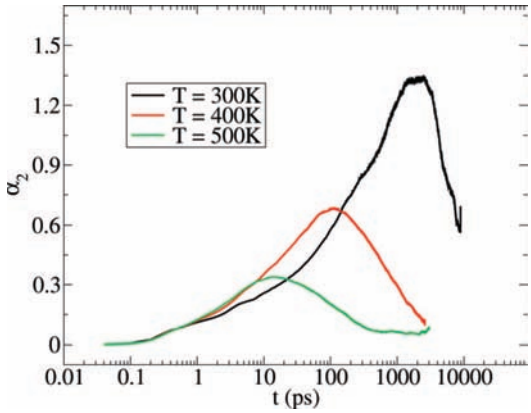

FIGURE 2. Non-Gaussian parameter α_2 for the [BMIM$^+$] cation in [BMIM$^+$][PF6$^-$] at three different temperatures. At 300 K, the maximum of α_2 is at $t^* = 2.48$ ns, whereas at 400 K, it shifts to 109 ps.

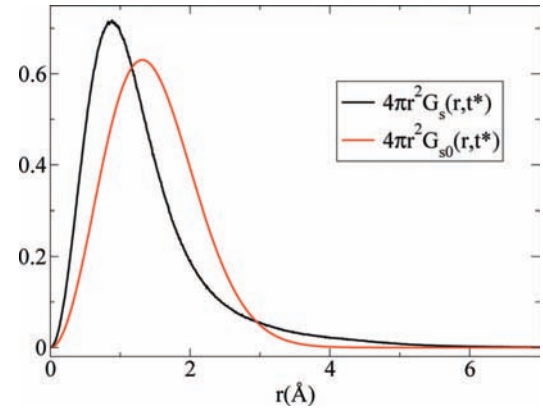

FIGURE 3. Self part of the van Hove correlation function for the cations and its standard Gaussian form at the time $t^* = 2.48$ ns when α_2 reaches its maximum deviation from the Gaussian behavior for ([BMIM$^+$][PF6$^-$]) at 300 K. Because this system is isotropic, we only consider the radial part $4\pi r^2 G_s(\mathbf{r},t^*)$. Reproduced with permission from ref 36. Copyright 2006, The National Academy of Sciences of the U.S.A.

scale. All liquids display ballistic motion at short time and approach a Gaussian diffusive behavior when time goes to infinity. Therefore, the relevant issue is the time scale on which ILs display non-Gaussian diffusivity. This is important because, as we will show, this time scale often coincides with that for chemical and photochemical reactivity. A direct way to answer this question is to compute the self part of the van Hove correlation function defined as[33]

$$G_s(\mathbf{r}, t) = \frac{1}{N}\left\langle \sum_{i=1}^{N} \delta\left(r - \left|\mathbf{r}_i(t) - \mathbf{r}_i(0)\right|\right)\right\rangle \qquad (1)$$

The self part of the van Have correlation function describes the diffusion of a particle, which for a normal liquid satisfies Fick's equation with an initial condition of the delta function. For an isotropic system, $4\pi r^2 G_s(\mathbf{r},t)\,dr$ is the probability of finding at time t an ion in the vicinity dr of points at the distance r given that initially the ion was located at the origin.

One can easily prove that the solution of Fick's diffusion equation is the standard Gaussian function

$$G_{s0}(\mathbf{r}, t) = \left[\frac{3}{2\pi\langle r^2(t)\rangle}\right]^{\frac{3}{2}} e^{-\frac{3r^2}{2\langle r^2(t)\rangle^2}} \qquad (2)$$

This solution is what one usually obtains for normal liquids, in which, after a short inertial response, Brownian dynamics is established. Supercooled or glassy systems display much longer tails in the distribution.

It is possible to compute the different moments of $G_s(\mathbf{r},t)$. In particular, for a Gaussian distribution, only even moments are different from 0. To compare the deviation of $G_s(\mathbf{r},t)$ from $G_{s0}(\mathbf{r},t)$, it is customary to analyze the behavior of the non-Gaussian parameter,[34,35] $\alpha_2(t) = 3/5(\langle r^4(t)\rangle/\langle r^2(t)\rangle^2) - 1$. Only when diffusion is Gaussian is $\alpha_2(t)$ identically equal to 0.

Figure 2 shows the non-Gaussian parameter as a function of time at three different temperatures. At 300 K, α_2 displays its maximum on a time scale (t^*) of nanoseconds. This maximum dramatically decreases and shifts to shorter times when the temperature is increased.[36]

We computed the self van Hove correlation function and the standard Gaussian function at the time of maxima deviation t^* for 1-butyl-3-methylimidazolium hexafluorophosphate [BMIM$^+$][PF6$^-$] at 300 K. Figure 3 clearly indicates that most ions diffuse slower than expected from Fick's law; however, a group of ions exist that diffuse much faster. This can be appreciated from the fact that in Figure 3 $G_s(\mathbf{r},t^*)$ and $G_{s0}(\mathbf{r},t^*)$ cross at a distance of approximately 2.9 Å after which $G_s(\mathbf{r},t^*)$ has a much longer tail than the corresponding Gaussian function $G_{s0}(\mathbf{r},t^*)$.

Furthermore, as it is usually the case for glassy or supercooled liquids,[37] it is possible to discriminate between ensembles of ions that are diffusing at slower and faster rates. We found that subensembles of particles that diffuse at slow rates and subensembles of particles that move at fast rates are correlated in space. Radial distribution functions within the fast subensemble or within the slow subensemble display maxima at contact distances, while the cross-distribution functions show a depletion in density at a contact distance. An interesting result is that within the diffusively fast subensemble $G_s(\mathbf{r},t)$ shows multiple peaks. These multiple peaks shown in parts a and c of Figure 4 are usually indicative of diffusion through hopping mechanisms.[38]

The slow dynamics of the solvent gives rise to a very interesting phenomenon: The existence of locally heterogeneous environments on a time scale relevant to chemical reactivity and optical spectroscopy. These local environments are not necessarily related to polar/nonpolar regions of the liquid but, instead, may correspond to generic environments that do not significantly change on a time scale relevant to chemical reactivity. In other words, chemical or photochemical processes that take place on a several nanosecond time scale most likely occur in environments in which local solvent averaging does not significantly take place.

The manifestation of this local solvent heterogeneity is most obvious in the experiments of Samanta and coworkers,[17] where an absorption wavelength-dependent

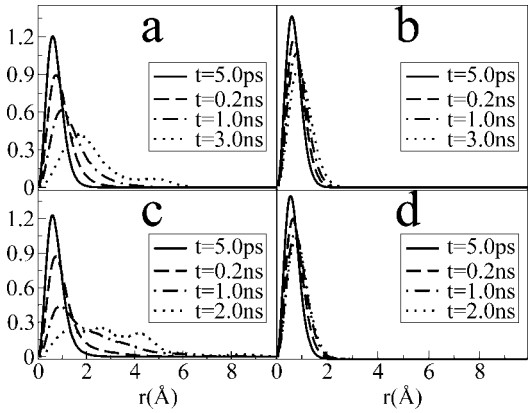

FIGURE 4. Self part of the van Hove correlation function $G_s(\mathbf{r},t)$ for anions (a and b) and cations (c and d) in the mobile ensemble (a and c) and the immobile ensemble (b and d) at four different times. Reproduced with permission from ref 36. Copyright 2006, The National Academy of Sciences of the U.S.A.

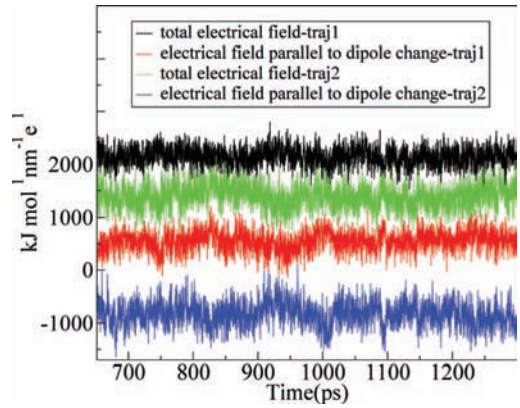

FIGURE 5. Absolute value of the electric field generated by the solvent at the location of one of the carbon atoms close to the center of mass of ANF and the projection of this electric field onto the direction of the ground to excited state dipole moment change $\vec{\Delta\mu}$ as a function of time for two different trajectories. As can be appreciated, the projection of the electric field onto $\vec{\Delta\mu}$ is different in each trajectory but nearly constant with respect to time. This phenomenon of constancy with respect to time and variation with respect to space is the cause for the experimentally observed REE. Reproduced with permission from ref 36. Copyright 2006, The National Academy of Sciences of the U.S.A.

emission spectrum is observed upon electronic photo-excitation of 2-amino-7-nitrofluorene (ANF) in different solvents.

Red Edge Effects: Local Heterogeneity on Time Scales Relevant to Photochemical Reactivity

Red edge effects are commonly observed for systems in which the excited state of the probe is not fully equilibrated with the solvent on the time scale of emission[39–50] (see for example the excellent review article by Demchenko).[40]

It is clear that this phenomenon can arise because of two different causes. Environments that display "quasi-permanent" structural heterogeneity (colloidal gels or micelles for example) or environments that are heterogeneous because solvent averaging is slow and occurs on a time scale longer than that required for the relevant chemical or photochemical process in question.

An extreme example of this slow dynamics can be observed for example upon excitation of tryptophan[45,51] residues in denatured proteins. In this case, local environments provided by nearby amino acids are different for each tryptophan and do not get averaged. One therefore observes a red edge effect upon electronic photo-excitation. In other words, the structure of the surrounding environment is different for each fluorescent probe, and these environments do not exchange on a time scale relevant to spectroscopy or chemical reactivity. Each tryptophan absorbs and emits at a slightly different wavelength, giving rise to a large broadening of the spectrum and to an absorption wavelength-dependent emission spectrum.

In the case of RTILs, we find that because of hindrance caused by the slow solvent dynamics the fluorescent probe can only freely rotate on a time scale that is much longer than its fluorescence lifetime. In a liquid composed of bulky organic cations and anions, the fluorescent probe molecule will experience significantly different local electric fields depending upon its relative orientation with respect to a fixed spatial set of axes. Furthermore, for an ensemble of reactive molecules in different solvent locations, these local electric fields will not average out to a common value on a time scale consistent with the excited state lifetime of the probes. In our recent study of ANF in a RTIL,[36] we followed the solvent electric field and the projection of this vector onto the ground to excited dipole moment change $\vec{\Delta\mu}$ as a function of time. We found from these studies that, as shown in Figure 5, both the electric field at the center of mass of the probe and the projection onto $\vec{\Delta\mu}$ are nearly constant throughout individual simulations but vary greatly across runs.

This clearly implies that solvent averaging of local environments does not fully occur on a nanosecond time scale. In our simulations, the ground to excited state gap was assumed to be solely determined by electrostatics. Consistent with Figure 5, we found that the values of the solute–solvent electrostatic energy were trajectory-dependent but almost time-independent.

After photo-excitation of the probe, an initial transient behavior was observed after which neither the electric field generated by the solvent nor its projection onto the dipole moment of the excited state probe significantly changed. We ascribe this behavior to the slow dynamics of the solvent and the hindered nature of the solute rotations.

On the basis of these studies, we conclude that because of the lack of adiabaticity in the response of the solvent upon photo-excitation of a solute probe (i.e., the inability of the solvent to promptly respond to a change in charge distribution of the probe on a time scale consistent with photo-emission), each molecule responds to a site-specific perturbation and absorbs and emits at a different wavelength.

The absorption wavelength-dependent behavior observed[17] for ANF in an ionic solvent can be satisfactorily described by performing an average over an ensemble of

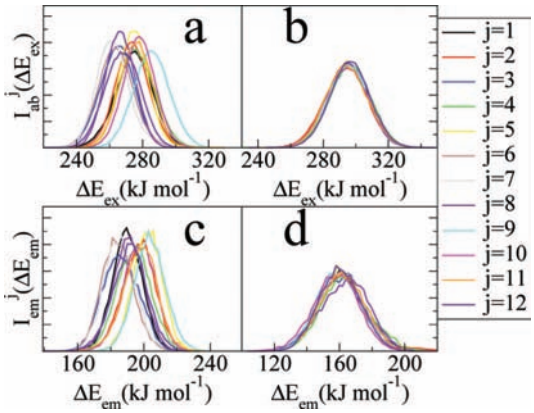

FIGURE 6. Overlayed are different curves that correspond to the spectrum of ANF in [BMIM$^+$][PF6$^-$] computed from each of our 12 molecular dynamics trajectories [absorption (a) and emission (c)] as well as in methanol [absorption (b) and emission (d)]. In the case of the IL, we observe site-specific spectra, whereas in methanol, all spectra are superimposable. Each of these individual spectra contributes to the total signal. Reproduced with permission from ref.[36] Copyright 2006, The National Academy of Sciences of the U.S.A.

molecular dynamics simulations. In this case, each trajectory is first equilibrated in the ground electronic state and then photo-excited into the first excited electronic state. Each trajectory therefore contributes an absorption and an emission spectrum, and the overall absorption wavelength-dependent emission of the system can be computed as the joint probability of ANF absorbing at λ_{abs} and emitting at λ_{emis}.[36,52]

We have computed absorption and emission spectra of ANF for trajectories with different initial conditions in [BMIM$^+$][PF6$^-$]. For the purpose of comparison, we have also performed identical simulations using methanol as a solvent. It is clear from Figure 6 that all spectra corresponding to different simulation systems superimpose in the case of methanol, while they are different in the case of the IL. This unique local behavior in the case of each trajectory is the underlying origin of the red edge effect observed by Samanta and co-workers.

If we analyze absorption and emission spectra for selected trajectories, we commonly find that those absorbing on the red edge also emit on the red edge. This result, which is shown in parts a and b of Figure 7, is a consequence of the slow dynamics of the solvent.

If solvent averaging around the exited-state molecule was fast compared to its fluorescence lifetime, then the Stokes shift for each trajectory would converge on the time scale of emission and the gap between excited and ground states would be independent of the initial local environment. In other words, the emission spectrum would be absoption wavelength-independent. Instead, because the Stokes shift is not converged and ANF emits from local environments that have a memory of the initial excitation solvent surrounding, it appears that molecules excited at high frequencies emit at higher energies, while those excited at lower frequencies emit at lower energies. Figure 7c shows the ensemble averaged absoption wavelength-dependent emission spectrum of ANF in the IL. Figure 7c closely coincides with the experimental results of Samanta and co-workers.

Figure 8 shows the maximum of emission as a function of the absorption wavelength derived from our simulations in the case of the IL and in methanol. It is clear that the absorption wavelength-dependent behavior is only present in the ionic system and is absent in the case of methanol.

The issue of whether permanent structural heterogeneity (such as in micelles and colloidal gels) is the underlying cause for the observed red edge effect (REE) or if the effect arises as a simple consequence of the high viscosity and slow dynamics of the liquid can start to be addressed if we look at the time-dependent version of Figure 8.

Figure 9 shows the time-dependent behavior of the absorption wavelength-dependent emission spectrum maximum as a function of the excitation wavelength. It is clear that for all curves independent of the absorption wavelength the maximum of emission shifts to smaller energies as time evolves, indicating that the Stokes shift is evolving toward equilibrium. It is also clear from Figure 9 that the absorption wavelength-dependent behavior is much more pronounced at short times than at long times, indicating that solvent averaging does occur on a longer time scale.

From these results, we conclude that the locally heterogeneous environments responsible for the REE are a consequence of the loss of ergodicity on a time scale similar or longer than the lifetime of the probe. This result does not negate the existence of permanent polar and nonpolar regions in these complex solvents, but it is clear that, because the absorption wavelength-dependent phenomena disappears on a longer time scale, these can not be responsible for the red edge effect. It is possible however that the lifetime of recently reported polar and nonpolar regions in these solvents may be similar to the time upon which we observe the absorption wavelength-dependent phenomena disappear. If this was the case, then the nature of these structures must be quite different from that of micelles, which are very long lived. As far as we know, the lifetime of these regions have not yet been reported either experimentally or computationally, and consequently, the role of them in the time-dependent spectroscopic phenomena is still unclear.

The Problem of Computing the Viscosity of RTILs

The high viscosity of RTILs is intrinsically related to the red edge effect and the loss of ergodicity on certain time scales.[7,8,53] In fact, viscosity is one of the most important properties to consider in practical applications involving RTILs. Viscosity coefficients have been measured for different ILs,[15,54–59] and solvents can be found with a wide range of viscosity values. The most common room-temperature ionic solvents have viscosities reported to be between 2 and 4 orders of magnitude larger than that of room-temperature water.

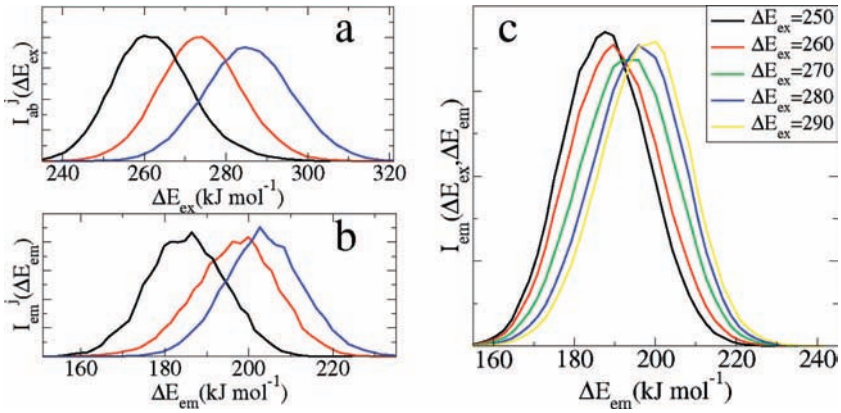

FIGURE 7. (a) Absorption spectra of ANF in [BMIM$^+$][PF6$^-$] computed from three independent molecular dynamics trajectories. (b) Emission spectra from the same three trajectories. (c) Ensemble averaged steady-state fluorescence spectra of ANF as a function of the excitation energy at room temperature in [BMIM$^+$][PF6$^-$]. Reproduced with permission from ref 52. Copyright 2006, American Chemical Society.

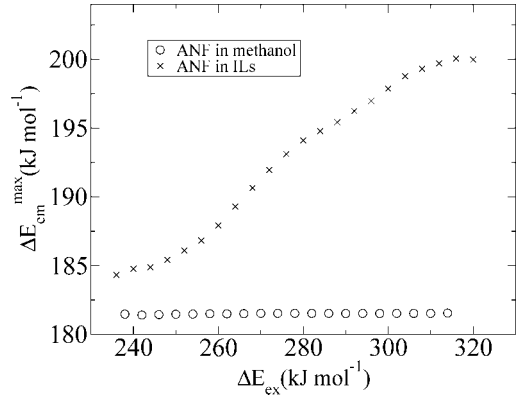

FIGURE 8. Maximum of emission ΔE_{em} as a function of the excitation wavelength for ANF in [BMIM$^+$][PF6$^-$] (×) and methanol (○) from our computer simulations in ref 36. The excited-state lifetime of ANF is 100 ps. Reproduced with permission from ref 36. Copyright 2006, The National Academy of Sciences of the U.S.A.

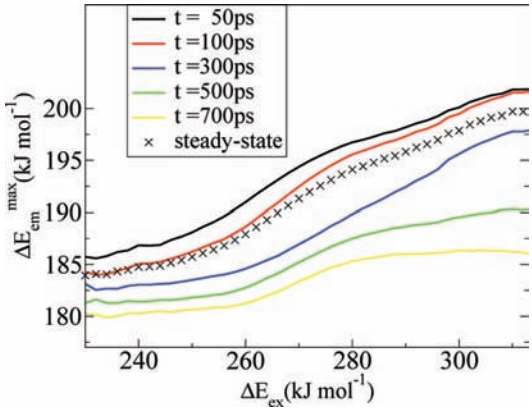

FIGURE 9. Same as Figure 8, except that emission maxima are computed at five different times. The steady-state result shown in Figure 8 is also shown here as ×. Adapted with permission from ref 52. Copyright 2006, American Chemical Society.

Both experiments and theory encounter significant difficulties upon establishing accurate values for viscosity coefficients of RTILs. In the case of experiments, this is because small amounts of halogen or water contaminants can significantly change the values measured. In the case of atomistic simulations, it is very challenging to compute viscosity coefficients for systems that are highly viscous. This is because the hydrodynamic limit where the experimental data are measured is extremely difficult to reach. Convergence requires simulation box sizes that are many times beyond current computational capabilities. Several theoretical studies have partially addressed the problem of viscosity in ILs.[60–62] However, a complete microscopic description of viscosity in ILs is still missing. In a recent paper,[63] we have attempted to address this problem in detail, making contact between macroscopic hydrodynamic predictions and the linear response theory.[63]

Common computational approaches to calculate viscosities are usually based on the evaluation of the transverse current autocorrelation function (an equilibrium property of the system) or nonequilibrium schemes, where a velocity or acceleration profile is introduced to the system (see ref 63 and citations therein). The problem with the equilibrium approach to compute the viscosity $\eta(k)$ is that it requires a highly accurate integral with respect to time of the transverse current autocorrelation function[63]

$$\eta(k) = \frac{\rho}{k^2}\frac{C(k, t=0)}{C(k, \omega=0)} \tag{3}$$

where

$$C(k, \omega=0) = \int_0^\infty C(k, \tau)\mathrm{d}\tau \tag{4}$$

and

$$C(k, t) = \langle \sum_{\mathrm{q}} m_{\mathrm{q}} v_{\mathrm{q}x} \mathrm{e}^{-ikz} \sum_{\mathrm{p}} m_{\mathrm{p}} \mathrm{v}_{\mathrm{p}x} \mathrm{e}^{ikz} \rangle \tag{5}$$

is the transverse current autocorrelation function. Here, q and p are particle indexes, while m, v, and ρ are the corresponding particle masses, velocities, and system density, respectively. For simpler solvents (such as room-temperature water), this is not a problem because normal computer simulations are not far from the hydrodynamic limit. We found that this is not the case for RTILs. We have performed extensive simulations of 1-hexyl-3-methylimidazolium chloride ([HMIM$^+$][Cl$^-$]) using a system size of more than 260 000 atoms, corresponding to a box size of more than 30 nm in length. To the best of our knowledge, these are the largest atomistic simulations of

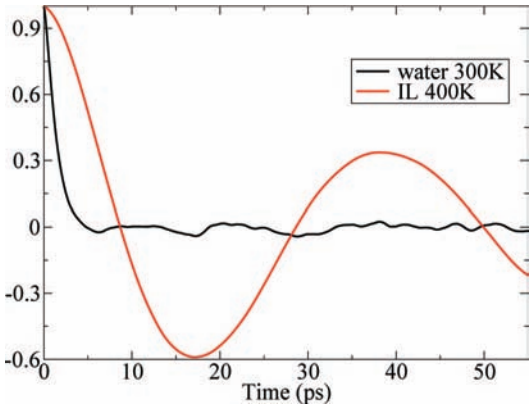

FIGURE 10. Transverse current autocorrelation function for water at 300 K and [HMIM$^+$][Cl$^-$] at 400 K. The correlation function shows a large negative minimum in the case of IL but not in the case of water. The *z* direction length was 5 nm in the case of water and 30.2 nm in the case of the IL.

ILs currently available in the literature.[63] Figure 10 shows a comparison between $C(k,t)$ for water and [HMIM$^+$][Cl$^-$].

To estimate the viscosity coefficient, two limits must be reached: $k = 0$ (infinite system), and $\omega = 0$ (infinite time). As we can see from Figure 10, our very large IL system shows a deep minimum at around 17 ps, which is indicative of strong non-hydrodynamic behavior[33] (i.e., $k \neq 0$). Therefore, the infinite system limit has not been reached. Furthermore, Figure 10 shows that at this value of k temporal correlations last for significantly long times. The zero frequency value of $C(k,\omega = 0)$ is therefore also unavailable because the computation of $C(k,t)$ for long t values is prohibitive. Instead, the result for water does not show these complications, and the corresponding time correlation function can be easily integrated to obtain a reasonable value for the viscosity coefficient.[64] Clearly, this equilibrium method is not viable for these types of IL systems at room temperature.

Several nonequilibrium schemes can be devised to study the viscosity of liquids (see ref 63 and citations therein). In one of these schemes, one establishes a periodic acceleration drag and studies the resulting velocity profile as a function of the acceleration wavenumbers.[63]

When an acceleration profile of the form

$$a_x(z, t) = a_0 \cos(kz) \tag{6}$$

is imposed on the system, the Navier-Stokes equation predicts a velocity profile of the form

$$u_x(z, t) = a_0\tau(1 - e^{-t/\tau})\cos(kz) \tag{7}$$

In our recently developed linear response approach, $(1 - e^{-t/\tau})$ is replaced by an integral over the tranverse current autocorrelation function.[63] The long time behavior of this function is $u_x(z,t = \infty) = a_0\tau \cos(kz) = u_0 \cos(kz)$, where the relaxation time τ is defined as $\tau = \rho/\eta k^2$. In the linear response approach, this result is still valid but η is a function $\eta(k)$. Therefore, when the steady-state velocity profile is fitted to a $\cos(kz)$ form, from the amplitude u_0, one can obtain the viscosity coefficient $\eta(k)$. A Newtonian liquid is such that $\eta(k)$ is independent of a_0. The wavenumbers that can be studied by computer simulations are bounded by the size of the simulation box. The larger the simulation box, the smaller the wavenumbers and the closer to the actual hydrodynamic limit. For most commonly studied liquids, the weak perturbation limit in which the viscosity (obtained from the amplitude of the velocity profile) is independent of the perturbation strength is easy to reach. Figure 11 shows how this is the case for room-temperature water.

Parts a and b of Figure 11 correspond to two simulations with imposed drag acceleration values $a_0 = 0.04$ and 0.08 nm/ps^2. The corresponding amplitudes of the velocity profiles after a transient initial period are 0.062 and 0.126 nm/ps. Clearly, a_0 and u_0 are proportional, and a value of the viscosity coefficient can be established. Therefore, these simulations confirm that for the perturbation wavenumbers used water behaves in a Newtonian fashion.

A very different result is obtained in the case of the IL at 400 K, as can be appreciated in Figure 12.

Even though the box size is much larger in the case of the IL and the corresponding wavenumber is much smaller, this system behaves in a non-Newtonian fashion. For drag accelerations of $a_0 = 0.01$ and 0.02 nm/ps^2, which are much smaller than those imposed in the case of water, we have observed that not only a_0 and u_0 are not proportional but also the velocity profile at the higher drag rate does not have a $\cos(kz)$ form. The velocity profile at $a_0 = 0.02$ nm/ps^2 is very similar to that found in polymer melts. Imposing an acceleration perturbation of a single given wavenumber results in a velocity profile that is flat! This corresponds to the breakdown of the linear response theory. This result with wide potential implications in the analytical separation field implies a behavior that is highly nonlinear because a given acceleration frequency results in an infinite linear combination of velocity frequencies. We conclude that for wavenumbers consistent with a length scale of several tens of nanometers the flow of some ILs is non-Newtonian, and we expect this behavior to be present if these liquids are forced to flow in micro/nanofluidic devices.

It is interesting to emphasize that usual simulations in which only a few hundred cations and anions are used may pose an important problem in the calculation of viscosities using drag accelerations. This is because the allowed acceleration wavenumbers compatible with the box size are similar to the frequencies relevant in the radial distribution functions of the liquid. This implies that forcing flow on such small systems will cause liquid structure deformation. We have observed this distortion in our simulations of small systems.

By analyzing the long time steady-state response of the IL, we have established that the linear response theory breaks down for perturbations such as in Figure 12. It is interesting to investigate the transient response of these systems as compared to linear response predictions.

This can be achieved by analyzing the transient behavior of the function $\langle V(t)\rangle$ defined as

$$V(t) = \sum_{q} 2m_q v_{qx}(t)\cos(kz_q(t))/M$$

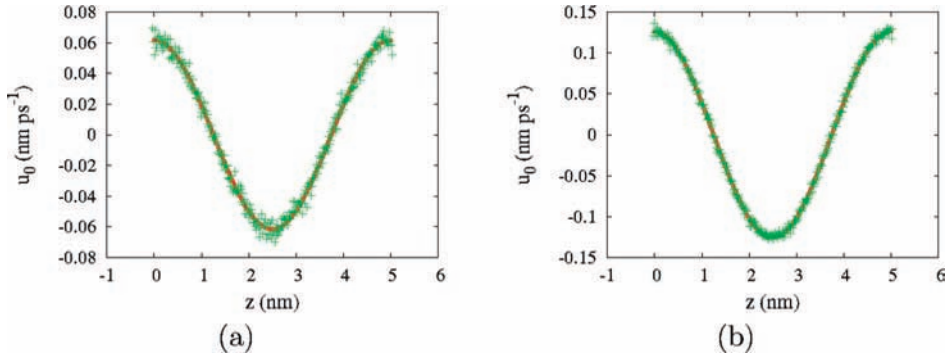

FIGURE 11. Velocity profiles for simulations with different externally imposed drag accelerations in the case of room-temperature water. (a) $a_0 = 0.04$ nm/ps^2, and (b) $a_0 = 0.08$ nm/ps^2. The length of our simulation box is 5 nm. The thermal speed of water at $T = 300$ K is approximately 0.6 nm/ps in each Cartesian coordinate. The weak perturbation imposed here induces a response that is linear.

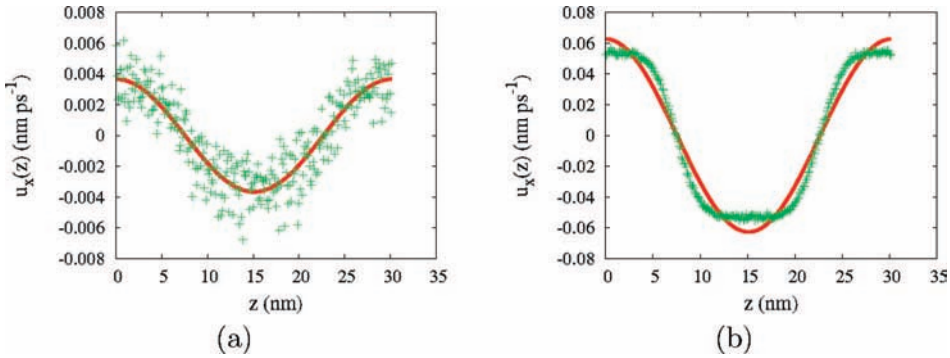

FIGURE 12. Same as Figure 11 but in the case of [HMIM$^+$][Cl$^-$] at 400 K. (a) $a_0 = 0.01$ nm/ps^2, and (b) $a_0 = 0.02$ nm/ps^2. The box length here is 30.2 nm. The thermal speed of IL at $T = 400$ K is close to 0.7 nm/ps in each Cartesian direction. Although the relative perturbation is much weaker than in the case of water, the system responds nonlinearly. Adapted with permission from ref 63. Copyright 2007, American Chemical Society.

where $M = \sum_q m_q$. We have recently shown that if the linear response theory is valid then

$$\frac{\langle V(t)\rangle}{a_0} = \int_0^t \frac{C(k,\tau)}{C(k,t=0)}\mathrm{d}\tau \qquad (8)$$

The left hand side of eq 8 is a nonequilibrium time average, while the right hand side is an integral over an equilibrium time correlation function. These two quantities can be separately computed from nonequilibrium and equilibrium simulations. Figure 13 shows a comparison between $\langle V(t)\rangle/a_0$ (red and green correspond to different values of a_0) and the integral on the right hand side of eq 8 (black). The left hand side of the equation corresponds to the transient velocity profile obtained upon applying a periodic drag perturbation. It is obviously clear that at times beyond 10 ps $\langle V(t)\rangle/a_0$ is not a constant function independent of a_0. Therefore, for longer times, linear response theory breaks and the fluctuation dissipation theorem does not apply. Even for small accelerations, such as the ones imposed in this study, the system behaves in a nonlinear fashion. It is clear now why one is not able to obtain an acceleration drag-independent viscosity coefficient from the periodic perturbation method because this method relies on the validity of linear response theory at long times when the velocity profile is time-independent.

Even though we have shown that different computational approaches cannot reach the macroscopic limit in which the viscosity coefficient is measured, it is interesting to know what the best viscosity predictions are based on our largest simulation system and our smallest applied

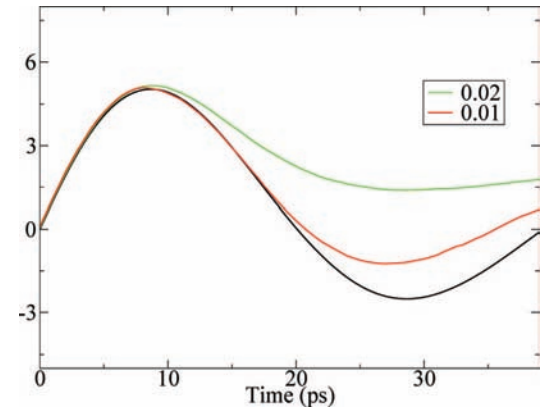

FIGURE 13. Transient response of the IL under external perturbations at 400 K. The solid black line corresponds to the integral as a function of time t of the equilibrium autocorrelation function, while the other curves correspond to the normalized instantaneous velocity amplitudes established upon application of different external accelerations, a_0. $k = 0.208$ nm^{-1}. Adapted with permission from ref 63. Copyright 2007, American Chemical Society.

drag perturbation. To match the temperatures at which our simulations were carried out, we fitted the data in ref 59 to the Vogel–Fulcher–Tammann equation

$$\eta = \eta_0 \mathrm{e}^{\frac{B}{T-T_0}}$$

The viscosity obtained by extrapolating the experimental data to 400 K is 26.7×10^{-3} kg m^{-1} s^{-1}, while the prediction obtained from the periodic perturbation method is

51.0×10^{-3} kg m^{-1} s^{-1}. These values are only a factor of 2 apart. Therefore, computer simulations appear to be able to deliver reasonable predictions of viscosity factors. The variability in force-field parameters, the use or lack of use of polarization, and the need to perform extremely large computer simulations are still important issues to be considered when attempting to carry out such calculations for RTILs.

Conclusions

Here, we have described some of the reasons why RTILs are exciting new solvents and the challenges that we and other groups face as we try to unravel their complex structure, fluid dynamics, and response upon perturbations. We find that the red edge effect, the non-Newtonian behavior on a nano- or sub-micrometer scale, and the existence of locally heterogeneous environments on a time scale relevant to chemical and photochemical reactivity are intimately married to the viscous and highly structured nature of these compounds. These properties make ILs different from most conventional solvents. We have made good progress in understanding these phenomena and hope to develop in the future means to harness the potential of these properties as effective tools to control the outcome of chemical and photochemical reactions.

Funding for different parts of this project has been provided by the National Science Foundation (CAREER 0547640), the American Chemical Society Grant PRF-G 41450-G6, and the University of Iowa Grant MSFP 85022915 awarded to C.J.M.

References

(1) Larsen, A. S.; Holbrey, J. D.; Tham, F. S.; Reed, C. A. Designing ionic liquids: Imidazolium melts with inert carborane anions. *J. Am. Chem. Soc.* **2000**, *122*, 7264–7272.
(2) Holbrey, J. D.; Reichert, W. M.; Nieuwenhuyzen, M.; Johnston, S.; Seddon, K. R.; Rogers, R. D. Crystal polymorphism in 1-butyl-3-methylimidazolium halides: Supporting ionic liquid formation by inhibition of crystallization. *Chem. Commun.* **2003**, 1636–1637.
(3) Ramos, J. J. M.; Afonso, C. A. M.; Branco, L. C. Glass transition relaxation and fragility in two room temperature ionic liquids. *J. Therm. Anal. Calorim.* **2003**, *71*, 659–666.
(4) Wilkes, J. S. Properties of ionic liquid solvents for catalysis. *J. Mol. Catal. A: Chem.* **2004**, *214*, 11–17.
(5) Holbrey, J. D.; Seddon, K. R. Ionic liquids. *Clean Technol. Environ. Policy* **1999**, *1*, 223–236.
(6) Forsyth, S. A.; Pringle, J. M.; MacFarlane, D. R. Ionic liquids—An overview. *Aust. J. Chem.* **2004**, *57*, 113–119.
(7) Ito, N.; Arzhantsev, S.; Maroncelli, M. The probe dependence of solvation dynamics and rotation in the ionic liquid 1-butyl-3-methyl-imidazolium hexafluorophosphate. *Chem. Phys. Lett.* **2004**, *396*, 83–91.
(8) Ingram, J. A.; Moog, R. S.; Ito, N.; Biswas, R.; Maroncelli, M. Solute rotation and solvation dynamics in a room-temperature ionic liquid. *J. Phys. Chem. B* **2003**, *107*, 5926–5932.
(9) Arzhantsev, S.; Maroncelli, M. Design and characterization of a femtosecond fluorescence spectrometer based on optical Kerr gating. *Appl. Spectrosc.* **2005**, *59*, 206–220.
(10) Antony, J. H.; Mertens, D.; Dolle, A.; Wasserscheid, P.; Carper, W. R. Molecular reorientational dynamics of the neat ionic liquid 1-butyl-3-methylimidazolium hexafluorophosphate by measurement of C-13 nuclear magnetic relaxation data. *ChemPhysChem* **2003**, *4*, 588–594.
(11) Ozawa, R.; Hayashi, S.; Saha, S.; Kobayashi, A.; Hamaguchi, H. Rotational isomerism and structure of the 1-butyl-3-methylimidazolium cation in the ionic liquid state. *Chem. Lett.* **2003**, *32*, 948–949.
(12) Chakrabarty, D.; Seth, D.; Chakraborty, A.; Sarkar, N. Dynamics of solvation and rotational relaxation of coumarin 153 in ionic liquid confined nanometer-sized microemulsions. *J. Phys. Chem. B* **2005**, *109*, 5753–5758.
(13) Every, H. A.; Bishop, A. G.; MacFarlane, D. R.; Oradd, G.; Forsyth, M. Transport properties in a family of dialkylimidazolium ionic liquids. *Phys. Chem. Chem. Phys.* **2004**, *6*, 1758–1765.
(14) Tokuda, H.; Hayamizu, K.; Ishii, K.; Susan, M. A. B. H.; Watanabe, M. Physicochemical properties and structures of room temperature ionic liquids. 1. Variation of anionic species. *J. Phys. Chem. B* **2004**, *108*, 16593–16600.
(15) Tokuda, H.; Hayamizu, K.; Ishii, K.; Susan, M. A. B. H.; Watanabe, M. Physicochemical properties and structures of room temperature ionic liquids. 2. Variation of alkyl chain length in imidazolium cation. *J. Phys. Chem. B* **2005**, *109*, 6103–6110.
(16) Umecky, T.; Kanakubo, M.; Ikushima, Y. Self-diffusion coefficients of 1-butyl-3-methylimidazolium hexafluorophosphate with pulsed-field gradient spin-echo NMR technique. *Fluid Phase Equilib.* **2005**, *228*, 329–333.
(17) Mandal, P. K.; Sarkar, M.; Samanta, A. Excitation-wavelength-dependent fluorescence behavior of some dipolar molecules in room-temperature ionic liquids. *J. Phys. Chem. A* **2004**, *108*, 9048–9053.
(18) Giovambattista, N.; Mazza, M. G.; Buldyrev, S. V.; Starr, F. W.; Stanley, H. E. Dynamic heterogeneities in supercooled water. *J. Phys. Chem. B* **2004**, *108*, 6655–6662.
(19) Ohmine, I.; Tanaka, H. Fluctuation, relaxations, and hydration in liquid water—Hydrogen-bond rearrangement dynamics. *Chem. Rev.* **1993**, *93*, 2545–2566.
(20) Sciortino, F.; Geiger, A.; Stanley, H. E. Network defects and molecular mobility in liquid water. *J. Chem. Phys.* **1992**, *96*, 3857–3865.
(21) Sciortino, F.; Geiger, A.; Stanley, H. E. Effect of defects on molecular mobility in liquid water. *Nature* **1991**, *354*, 218–221.
(22) Cates, M. E.; Fuchs, M.; Kroy, K.; Poon, W. C. K.; Puertas, A. M. Theory and simulation of gelation, arrest and yielding in attracting colloids. *J. Phys.: Condens. Matter* **2004**, *16*, S4861–S4875.
(23) Pham, K. N.; Puertas, A. M.; Bergenholtz, J.; Egelhaaf, S. U.; Moussaid, A.; Pusey, P. N.; Schofield, A. B.; Cates, M. E.; Fuchs, M.; Poon, W. C. K. Multiple glassy states in a simple model system. *Science* **2002**, *296*, 104–106.
(24) Puertas, A. M.; Fuchs, M.; Cates, M. E. Comparative simulation study of colloidal gels and glasses. *Phys. Rev. Lett.* **2002**, *88*, 098301.
(25) Puertas, A. M.; Fuchs, M.; Cates, M. E. Simulation study of nonergodicity transitions: Gelation in colloidal systems with short-range attractions. *Phys. Rev. E: Stat. Phys., Plasmas, Fluids, Relat.* **2003**, *67*, 031406.
(26) Puertas, A. M.; Fuchs, M.; Cates, M. E. Dynamical heterogeneities close to a colloidal gel. *J. Chem. Phys.* **2004**, *121*, 2813–2822.
(27) Wang, Y. T.; Voth, G. A. Unique spatial heterogeneity in ionic liquids. *J. Am. Chem. Soc.* **2005**, *127*, 12192–12193.
(28) Lopes, J. N. C.; Gomes, M. F. C.; Padua, A. A. H. Nonpolar, polar, and associating solutes in ionic liquids. *J. Phys. Chem. B* **2006**, *110*, 16816–16818.
(29) Margulis, C. J. Computational study of imidazolium-based ionic solvents with alkyl substituents of different lengths. *Mol. Phys.* **2004**, *102*, 829–838.
(30) Turner, M. B.; Spear, S. K.; Holbrey, J. D.; Rogers, R. D. Production of bioactive cellulose films reconstituted from ionic liquids. *Biomacromolecules* **2004**, *5*, 1379–1384.
(31) Remsing, R. C.; Swatloski, R. P.; Rogers, R. D.; Moyna, G. Mechanism of cellulose dissolution in the ionic liquid 1-*n*-butyl-3-methylimidazolium chloride: A C-13 and Cl-35/37 NMR relaxation study on model systems. *Chem. Commun.* **2006**, 1271–1273.
(32) Fort, D. A.; Remsing, R. C.; Swatloski, R. P.; Moyna, P.; Moyna, G.; Rogers, R. D. Can ionic liquids dissolve wood? Processing and analysis of lignocellulosic materials with 1-*n*-butyl-3-methylimidazolium chloride. *Green Chem.* **2007**, *9*, 63–69.
(33) Hansen, J. P.; McDonald, I. R. *Theory of Simple Liquids*; Academic Press: London, U.K., 1986.
(34) Sciortino, F.; Fabbian, L.; Chen, S. H.; Tartaglia, P. Supercooled water and the kinetic glass transition. 2. Collective dynamics. *Phys. Rev. E: Stat. Phys., Plasmas, Fluids, Relat.* **1997**, *56*, 5397–5404.
(35) Sciortino, F.; Gallo, P.; Tartaglia, P.; Chen, S. H. Supercooled water and the kinetic glass transition. *Phys. Rev. E: Stat. Phys., Plasmas, Fluids, Relat.* **1996**, *54*, 6331–6343.
(36) Hu, Z. H.; Margulis, C. J. Heterogeneity in a room-temperature ionic liquid: Persistent local environments and the red-edge effect. *Proc. Natl. Acad. Sci. U.S.A.* **2006**, *103*, 831–836.
(37) Kob, W.; Donati, C.; Plimpton, S. J.; Poole, P. H.; Glotzer, S. C. Dynamical heterogeneities in a supercooled Lennard–Jones liquid. *Phys. Rev. Lett.* **1997**, *79*, 2827–2830.

(38) Ribeiro, M. C. C. Translational and reorientational heterogeneity in the glass-forming liquid $Ca_{0.4}K_{0.6}(NO_3)_{1.4}$. *Phys. Chem. Chem. Phys.* **2004**, *6*, 771–774.
(39) Duportail, G.; Klymchenko, A.; Mely, Y.; Demchenko, A. P. On the coupling between surface charge and hydration in biomembranes: Experiments with 3-hydroxyflavone probes. *J. Fluoresc.* **2002**, *12*, 181–185.
(40) Demchenko, A. P. The red-edge effects: 30 years of exploration. *Luminescence* **2002**, *17*, 19–42.
(41) Ercelen, S.; Kazan, D.; Erarslan, A.; Demchenko, A. P. On the excited-state energy transfer between tryptophan residues in proteins: The case of penicillin acylase. *Biophys. Chem.* **2001**, *90*, 203–217.
(42) Demchenko, A. P.; Gallay, J.; Vincent, M.; Apell, H. J. Fluorescence heterogeneity of tryptophans in Na,K-ATPase: Evidences for temperature-dependent energy transfer. *Biophys. Chem.* **1998**, *72*, 265–283.
(43) Vincent, M.; Gallay, J.; Demchenko, A. P. Solvent relaxation around the excited-state of indole—Analysis of fluorescence lifetime distributions and time-dependence spectral shifts. *J. Phys. Chem.* **1995**, *99*, 14931–14941.
(44) Demchenko, A. P.; Apell, H. J.; Sturmer, W.; Feddersen, B. Fluorescence spectroscopic studies on equilibrium dipole-relaxational dynamics of Na,K-ATPase. *Biophys. Chem.* **1993**, *48*, 135–147.
(45) Demchenko, A. P.; Gryczynski, I.; Gryczynski, Z.; Wiczk, W.; Malak, H.; Fishman, M. Intramolecular dynamics in the environment of the single tryptophan residue in staphylococcal nuclease. *Biophys. Chem.* **1993**, *48*, 39–48.
(46) Gakamsky, D. M.; Demchenko, A. P.; Nemkovich, N. A.; Rubinov, A. N.; Tomin, V. I.; Shcherbatska, N. V. Selective laser spectroscopy of 1-phenylnaphthylamine in phospholipid-membranes. *Biophys. Chem.* **1992**, *42*, 49–61.
(47) Demchenko, A. P.; Sytnik, A. I. Site selectivity in excited-state reactions in solutions. *J. Phys. Chem.* **1991**, *95*, 10518–10524.
(48) Demchenko, A. P.; Sytnik, A. I. Solvent reorganizational red-edge effect in intramolecular electron-transfer. *Proc. Natl. Acad. Sci. U.S.A.* **1991**, *88*, 9311–9314.
(49) Demchenko, A. P. Red-edge-excitation fluorescence spectroscopy of single-tryptophan proteins. *Eur. Biophys. J. Biophys. Lett.* **1988**, *16*, 121–129.
(50) Demchenko, A. P.; Ladokhin, A. S. Red-edge-excitation fluorescence spectroscopy of indole and tryptophan. *Eur. Biophys. J. Biophys. Lett.* **1988**, *15*, 369–379.
(51) Fidy, J.; Laberge, M.; Ullrich, B.; Polgar, L.; Szeltner, Z.; Gallay, J.; Vincent, M. Tryptophan rotamers that report the conformational dynamics of proteins. *Pure Appl. Chem.* **2001**, *73*, 415–419.
(52) Hu, Z. H.; Margulis, C. J. A study of the time-resolved fluorescence spectrum and red edge effect of ANF in a room-temperature ionic liquid. *J. Phys. Chem. B* **2006**, *110*, 11025–11028.
(53) Chakrabarty, D.; Chakraborty, A.; Seth, D.; Sarkar, N. Effect of water, methanol, and acetonitrile on solvent relaxation and rotational relaxation of coumarin 153 in neat 1-hexyl-3-methylimidazolium hexafluorophosphate. *J. Phys. Chem. A* **2005**, *109*, 1764–1769.
(54) Huddleston, J. G.; Visser, A. E.; Reichert, W. M.; Willauer, H. D.; Broker, G. A.; Rogers, R. D. Characterization and comparison of hydrophilic and hydrophobic room temperature ionic liquids incorporating the imidazolium cation. *Green Chem.* **2001**, *3*, 156–164.
(55) Seddon, K. R.; Stark, A.; Torres, M. J. Influence of chloride, water, and organic solvents on the physical properties of ionic liquids. *Pure Appl. Chem.* **2000**, *72*, 2275–2287.
(56) Tokuda, H.; Ishii, K.; Susan, M. A. B. H.; Tsuzuki, S.; Hayamizu, K.; Watanabe, M. Physicochemical properties and structures of room-temperature ionic liquids. 3. Variation of cationic structures. *J. Phys. Chem. B* **2006**, *110*, 2833–2839.
(57) Shirota, H.; Castner, E. W. Why are viscosities lower for ionic liquids with $-CH_2Si(CH_3)_3$ vs $-CH_2C(CH_3)_3$ substitutions on the imidazolium cations? *J. Phys. Chem. B* **2005**, *109*, 21576–21585.
(58) Shirota, H.; Castner, E. W. Physical properties and intermolecular dynamics of an ionic liquid compared with its isoelectronic neutral binary solution. *J. Phys. Chem. A* **2005**, *109*, 9388–9392.
(59) Gomez, E.; Gonzalez, B.; Dominguez, A.; Tojo, E.; Tojo, J. Dynamic viscosities of a series of 1-alkyl-3-methylimidazolium chloride ionic liquids and their binary mixtures with water at several temperatures. *J. Chem. Eng. Data* **2006**, *51*, 696–701.
(60) Yan, T. Y.; Burnham, C. J.; Del Popolo, M. G.; Voth, G. A. Molecular dynamics simulation of ionic liquids: The effect of electronic polarizability. *J. Phys. Chem. B* **2004**, *108*, 11877–11881.
(61) Urahata, S. M.; Ribeiro, M. C. C. Collective excitations in an ionic liquid. *J. Chem. Phys.* **2006**, *124*, 74513.
(62) Rey-Castro, C.; Vega, L. F. Transport properties of the ionic liquid 1-ethyl-3-methylimidazolium chloride from equilibrium molecular dynamics simulation. The effect of temperature. *J. Phys. Chem. B* **2006**, *110*, 14426–14435.
(63) Hu, Z.; Margulis, C. J. On the response of an ionic liquid to external perturbations and the calculation of shear viscosity. *J. Phys. Chem. B* **2007**, *111*, 18, 4705–4714.
(64) Balucani, U.; Brodholt, J. P.; Jedlovszky, P.; Vallauri, R. Viscosity of liquid water from computer simulations with a polarizable potential model. *Phys. Rev. E: Stat. Phys., Plasmas, Fluids, Relat.* **2000**, *62*, 2971–2973.

AR700046M